CrossMark

Tunable Plasmonic Absorber Based on TiN-Nanosphere Liquid Crystal Hybrid in Visible and Near-Infrared Regions

Reza Rashiditabar[1] · Najmeh Nozhat[1] · Mohammad Sadegh Zare[1]

Abstract
In this paper, a tunable plasmonic absorber based on TiN-nanosphere/liquid crystal (LC) nanocomposite in visible and near-infrared regions is proposed. TiN-nanosphere/LC nanocomposite is a combination of titanium nitride (TiN) nanospheres dispersed in a host of LC and plays the main role in post fabrication tunability. The proposed absorber has three more than 90% absorption peaks and the absorption tunability of about 76 nm. It is shown that TiN-nanospheres are able to support localized surface plasmon resonance (LSPR). The Maxwell-Garnett theory is utilized to approximate the permittivity of the composite structure. Also, the effect of geometric parameters on the absorption is studied. Moreover, a single sheet of graphene is utilized to compensate the decrement of the absorption caused by the geometric parameters.

Keywords Plasmonics · Absorption · Effective medium theory · Liquid crystals · Surface plasmons · Resonance

Introduction

Electromagnetic absorbers are greatly utilized in different devices. There are different types of absorbers such as microwave [1], metamaterial (MTM) [2], and plasmonic absorbers [3]. The function of plasmonic absorbers is based on the surface plasmon polariton (SPP) or localized surface plasmon (LSP) [4, 5]. Plasmonic absorbers are widely proposed to be utilized in sensors [6], solar cells [7], modulators [8], switches [9], etc.

Absorption tunability has been a great consideration for many researchers [10], and in this case, liquid crystal (LC) has been widely chosen due to its flexible anisotropic property [11]. LC has been utilized in MTM [12] or plasmonic absorbers [13] to make a tunable absorber by applied electric field [14] or Argon laser if azo dye is added to LC to make an all optical tunable absorber [15]. Furthermore, liquid crystal can be used in different frequency regions. In [16], a microwave-tunable absorber has been proposed that can be tuned by external bias voltage applied to the LC. Shrekenhamer et al. have fabricated a single-band terahertz MTM absorber operating in 2–3.5-THz

region with the maximum absorption of 0.8 at 2.62 THz that is tunable about 0.12 THz by both frequency and voltage rate of the applied voltage [17]. A near-infrared tunable plasmonic absorber has been fabricated with two perfect absorption peaks and tunability of 30 nm [15]. A tunable plasmonic broadband absorber has been proposed that is sensitive to the size and angle of nanorods and LC acts as the host medium for nanorods to create a multi-resonance effective medium [13].

Effective medium has been a matter of discussion for many years and there have been many investigations to model the effective medium [18]. Maxwell-Garnett [19], Garcia [20], and Bruggman [21] are well-known methods to identify the effective parameters of the effective medium. Gao et al. have investigated the nonlinear behavior of silver-dielectric nanocomposite with effective permittivity variations under different applied electric filed as well as metal shape, volume fraction, and incident angle [22]. In [23], an effective medium has been fabricated to create large third-order susceptibility. Furthermore, the implementation of effective medium in birefringence material has been done in [24].

Graphene is a two-dimensional material with interesting optical properties, which can be utilized in different optoelectronic devices [25]. Graphene does not support SPP at visible and near-infrared wavelengths and its absorption is 2.3% as Nair et al. have measured it [26]. In addition, graphene is capable of supporting SPP at mid-infrared wavelengths [27, 28]. Therefore, there are graphene-based

✉ Najmeh Nozhat
  nozhat@sutech.ac.ir

[1] Department of Electrical Engineering, Shiraz University of Technology, Shiraz 7155713876, Iran
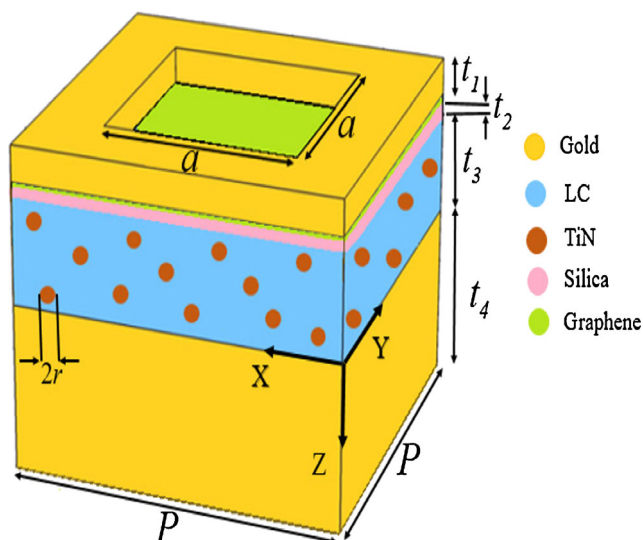
Fig. 1 The schematic view of the proposed absorber

plasmonic absorbers [29]. In [30], graphene is utilized to enhance the absorption due to the strong localized electric field caused by the magnetic resonances by the silver grating. Lu et al. have used graphene to enhance the absorption of ring groove structure in near-infrared region [31]. Zare et al. have proposed graphene-based plasmonic absorbers to improve absorption [32, 33].

In this work, a plasmonic absorber that consists of titanium nitride (TiN) nanospheres hosted by nematic LC has been proposed. It has been proved that TiN-nanospheres are capable of supporting localized surface plasmon resonance (LSPR) [34]. The proposed absorber has three near unity tunable absorption peaks in the wavelength range of 0.5 to 1.2 μm. Nematic type of LC is responsive to the applied voltage [14]. Hence, it can be a good candidate to make the proposed structure tunable. In addition, there are other geometric parameters to tune the structure with a strong absorption. In the proposed structure, the absorption tunability is enhanced to 76 nm. Also, there is an absorption peak in near-infrared

region which is enhanced to more than 90% as a single sheet of graphene is on the silica layer sandwiched between the top gold layer and the nanocomposite.

The paper is organized as follows. The geometry and characteristics of the proposed absorber is presented in "Structure Geometry and Materials" section. In "Simulation Procedure and Results" section, the simulation procedure is explained and the results are depicted. The paper is concluded in "Conclusion" section.

Structure Geometry and Materials

The unit cell of the proposed absorber is depicted in Fig. 1. The absorber is composed of TiN-nanospheres in the liquid crystal host medium that is sandwiched between two gold layers. There is a silica layer with a thickness of $t_2 = 5$ nm between the composite layer and the top gold layer. The gold substrate is thick enough with the thickness of $t_4 = 200$ nm to avoid any transmittance. The length of the top square aperture is $a = 150$ nm. The radius of nanospheres is $r = 10$ nm and the thicknesses of the top gold layer and the composite layer are $t_1 = 10$ nm and $t_3 = 100$ nm, respectively. The period of the structure is $P = 340$ nm and the unit cell is repeated along x- and y-axes.

The LC nanocomposite is a combination of nematic LC and TiN-nanospheres to create LSPR. Nematic LC is an anisotropic medium that its permittivity is described by a second rank tensor as the following formula [13]:

$$\varepsilon = \begin{pmatrix} \varepsilon_o\cos^2\phi + \varepsilon_e\sin^2\phi & 0 & (\varepsilon_o-\varepsilon_e)\sin\phi\cos\phi \\ 0 & \varepsilon_o & 0 \\ (\varepsilon_o-\varepsilon_e)\sin\phi\cos\phi & 0 & \varepsilon_e\cos^2\phi + \varepsilon_o\sin^2\phi \end{pmatrix} \quad (1)$$

where $\varepsilon_o = 3$ and $\varepsilon_e = 4$ are ordinary and extraordinary permittivities, respectively [35], when z-axis is considered as the reference. The tilt angle of the LC molecules is denoted by ϕ, which is the angle between the optical and z-axes in case the optical axis is in x-z plane. LC molecules are oriented
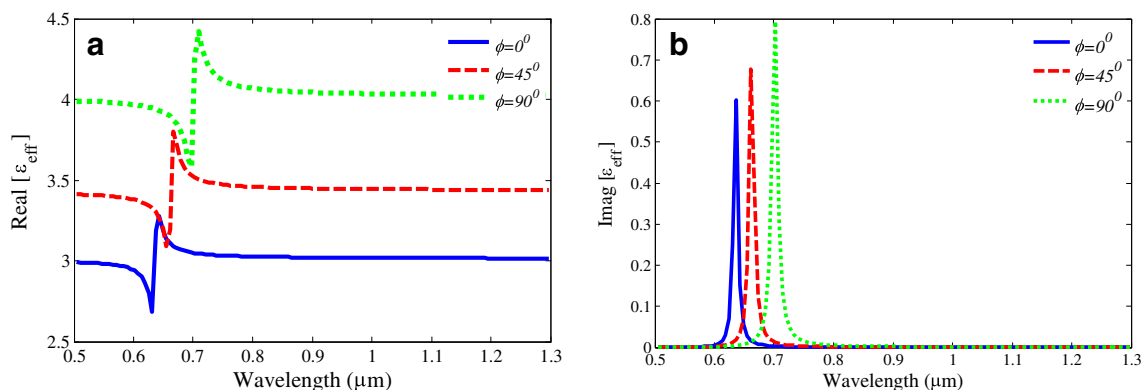

Fig. 2 The real (a) and imaginary (b) parts of the nanocomposite structure for different values of ϕ when $p = 0.001$
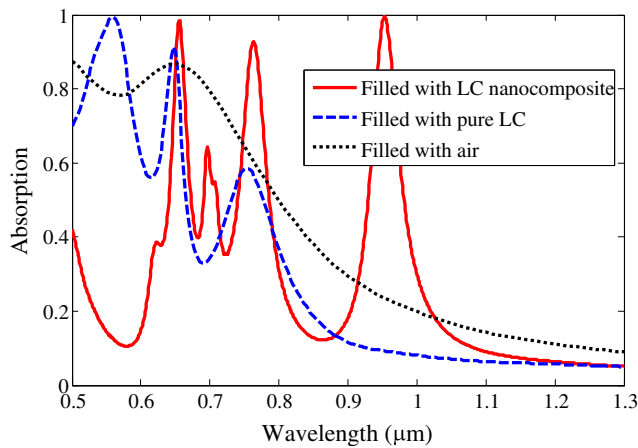
Fig. 3 Absorption spectra of the proposed structure filled with air, pure LC, and TiN-nanosphere/LC hybrid when $\phi = 90°$, $p = 0.001$, $a = 150$ nm, and $r = 10$ nm

according to the applied voltage. When liquid crystal is illuminated by a linearly polarized wave, it is possible to define an effective permittivity as below [36]:

$$\varepsilon_{\text{eff}} = \left(\frac{\cos^2 \phi}{\varepsilon_o} + \frac{\sin^2 \phi}{\varepsilon_e} \right)^{-1} \quad (2)$$

In the proposed absorber, the effective permittivity of the nanocomposite is analyzed and approximated by the Maxwell-Garnett formula. According to [37], the effective permittivity of the effective medium is given as follows:

$$\varepsilon_{\text{eff}} = \left(\frac{F}{3} \right) \left((1 + 2p) \varepsilon_{\text{TiN}} + 2(1 + p) \varepsilon_{\text{LC}} \right) \quad (3)$$

The local field factor (F) is defined as follows:

$$F = \frac{3\varepsilon_{\text{LC}}}{(\varepsilon_{\text{TiN}}(1-p) + \varepsilon_{\text{LC}}(2+p))} \quad (4)$$

where p is the volume fraction, ε_{LC} and ε_{TiN} are the LC and TiN-nanosphere permittivities, respectively. Moreover, Drude

model can describe the permittivity of TiN-nanospheres which is approximated as follows [38]:

$$\varepsilon_{\text{TiN}} = \varepsilon' + \left(\frac{\varepsilon'' + A\omega_p^2 V_F}{\omega^3 r} \right) \quad (5)$$

where ε' and ε'' are the real and imaginary parts of the bulk TiN permittivity, respectively. Johnson and Christy data are utilized to describe the bulk permittivities of gold [39] and TiN [40]. Also, Lemarchan data is used to describe the silica permittivity [41]. In Eq. (5), $\omega_p = 2.15 \times 10^{15}$ (rad/s) is the plasma frequency [42], $V_F = 1.39 \times 10^6$ (m/s) is the TiN Fermi velocity [43], r is the radius of TiN-nanospheres, and $A = 5$ is to show the additional damping of electron and the quantity is considered as mean free path of electron [38].

The real and imaginary parts of the effective permittivity of the nanocomposite structure for $\phi = 0°$, $\phi = 45°$, and $\phi = 90°$ are shown in Fig. 2.

Graphene is simulated by a sheet and characterized by the surface conductivity. According to Kubo formulation, the graphene conductivity is given as follows [44]:

$$\sigma_g(\omega, \mu_c, \Gamma, T) = \sigma_{intra} + \sigma_{inter}, \quad (6)$$

where σ_{intra} is the intraband electro-photon scattering that is described as the following:

$$\sigma_{intra} = -j \frac{e^2 k_B T}{\pi \hbar^2 (\omega - j2\Gamma)} \left[\frac{\mu_c}{k_B T} + 2\ln\left(\exp\left(-\frac{\mu_c}{k_B T} \right) + 1 \right) \right] \quad (7)$$

and σ_{inter} is the interband transition which is formulated as follows:

$$\sigma_{inter} = -j \frac{e^2}{4\pi \hbar} \ln\left[\frac{2|\mu_c| - (\omega - j2\Gamma)\hbar}{2|\mu_c| + (\omega - j2\Gamma)\hbar} \right] \quad (8)$$

Equation (8) is approximated when $k_B T << |\mu_c|$, $\hbar\omega$. $\hbar$, μ_c, and $\Gamma = 1/2\tau$ are reduced Planck constant, chemical potential, and phenomenological scattering rate, respectively. The momentum relaxation time is denoted by τ and T is temperature.

Fig. 4 (a) An array of TiN-nanospheres in LC with $r = 10$ nm, $a = 150$ nm, and $\phi = 90°$. (b) Electric field distribution of LSP resonance of TiN-nanospheres at $\lambda = 0.6$ μm
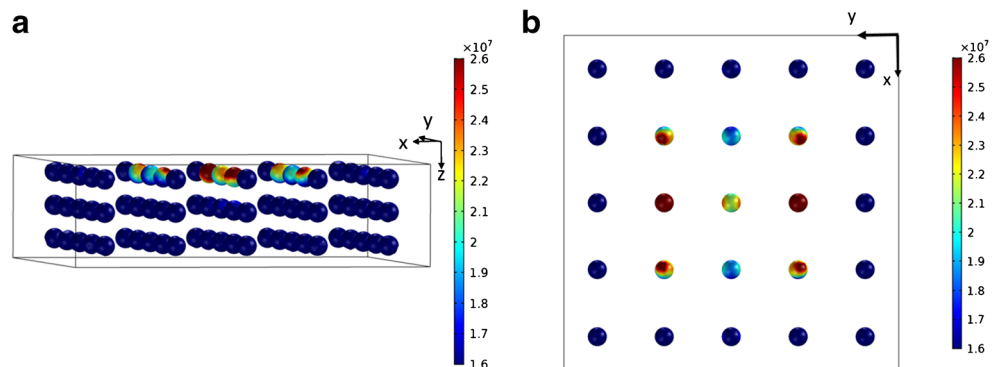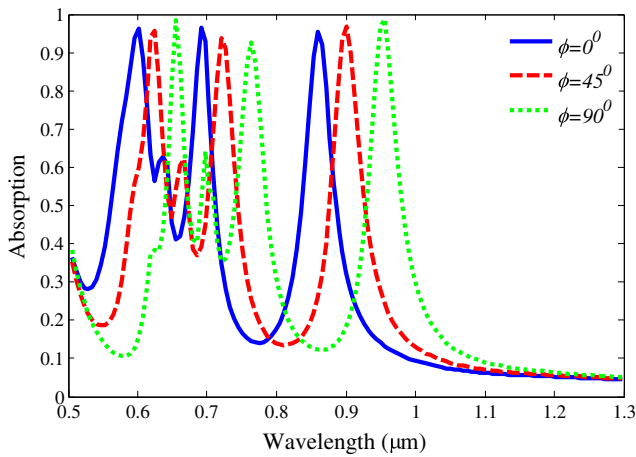
Fig. 5 Absorption spectra for different angles of LC optical axis ($\phi = 0°$, 45°, and 90°) as $p = 0.001$, $a = 150$ nm, and $r = 10$ nm

Fig. 7 The absorption spectra for different nanosphere radii when $\phi = 90°$, $a = 150$ nm, and $p = 0.001$

In our simulation, $T = 300$ K, $\mu_c = 0.15$ eV and $\Gamma = 0.659$ meV [45].

Simulation Procedure and Results

The finite element method (FEM) is utilized to calculate the absorption of the structure. The structure is illuminated normally by a plane wave along the z-axis and the periodic boundary condition (PBC) is applied along x- and y-axes. The absorption is calculated according to $A = 1 - R - T$, where T and R are the transmission and reflection powers, respectively. The absorption spectra of the proposed structure, when it is filled with air, pure LC, and TiN-nanosphere/LC hybrid, are shown in Fig. 3. It is obvious that without the nanocomposite structure, the absorption is low and there is no resonance in our desirable wavelength range. It is worth noting that by utilizing LC, three minor resonances appear in the analyzed wavelength region. The minor resonances are regarded as the intrinsic resonances of the structure. By
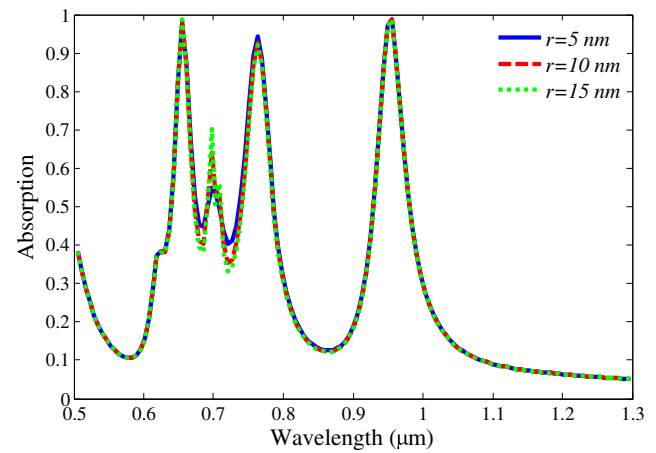
utilizing TiN-nanosphere/LC hybrid, three more than 90% absorption peaks appear at 0.66-, 0.76-, and 0.95-μm wavelengths, when $\phi = 90°$, $a = 150$ nm, $r = 10$ nm, and $p = 0.001$. The resonance of the TiN-nanosphere/LC hybrid is due to the LSPR on the surface of TiN-nanospheres. The electric filed distribution of TiN-nanospheres at the wavelength of 0.6 μm in the xy plane is shown in Fig. 4 that five TiN-nanospheres are in each row and the distance between the adjacent nanospheres is denoted by $d = 50$ nm. It is obvious that the LSP resonance of nanospheres near the aperture is more than the peripheral ones.

In order to show the tunability of the structure, the absorption spectra for different values of ϕ that is caused by the applied voltage are depicted in Fig. 5. It is obvious that by increasing ϕ, there is a red shift in the absorption spectrum. This phenomenon is in accordance with the red shift of the real and imaginary parts of the effective permittivity resonance of the Fig. 2. Therefore, the resonance of the structure depends on the resonance wavelength of the LC nanocomposite structure.
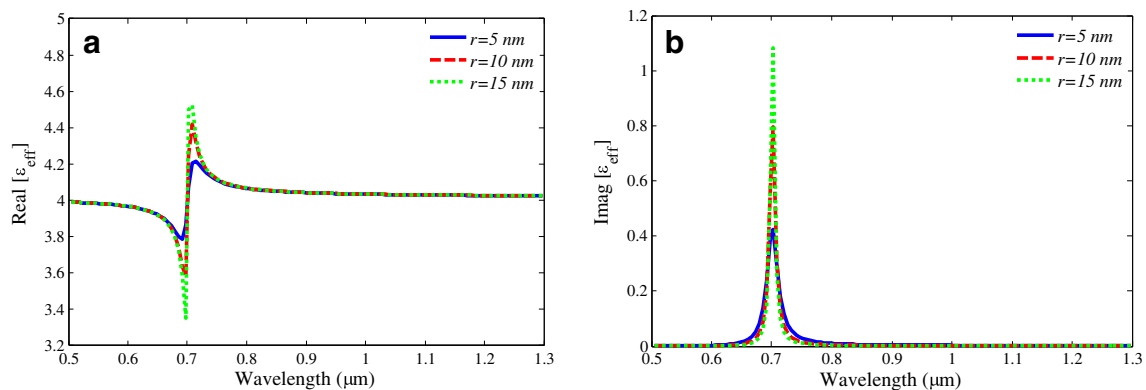

Fig. 6 The real (a) and imaginary (b) parts of the effective permittivity of TiN-nanosphere/LC hybrid for different nanosphere radii when $\phi = 90°$ and $p = 0.001$
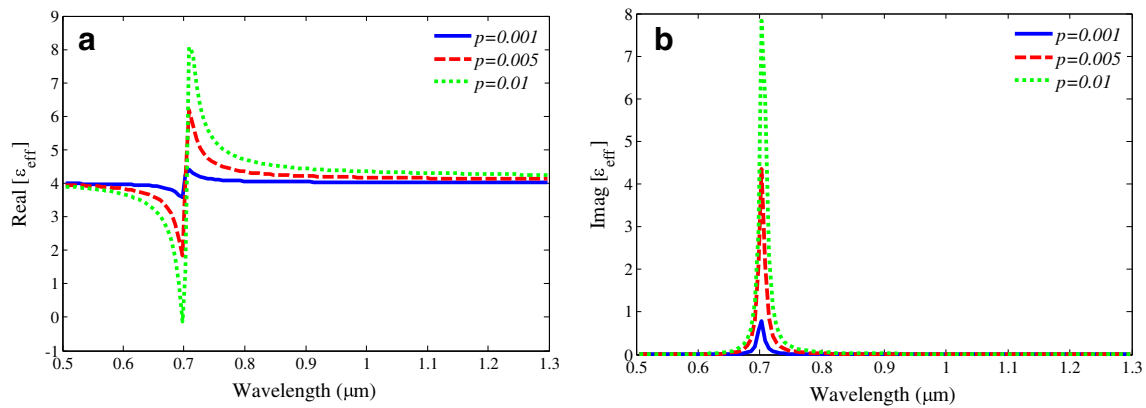
Fig. 8 The real (a) and imaginary (b) parts of the effective permittivity for volume fractions of $p = 0.001$, $p = 0.005$, and $p = 0.01$ as $\phi = 90°$ and $r = 10$ nm

In our simulations, the tunability of the absorption wavelength is 76 nm in average, which is fully controllable by the applied voltage and can be enhanced if the LC birefringence, $\Delta n(\theta) = n_e - n_o$, is chosen to be the maximum value [46]. When $\phi = 0°$, the absorption peaks are at $\lambda_1 = 0.6$ μm, $\lambda_2 = 0.69$ μm, and $\lambda_3 = 0.83$ μm, while the absorption peaks occur at $\lambda'_1 = 0.66$ μm, $\lambda'_2 = 0.76$ μm, and $\lambda'_3 = 0.95$ μm as $\phi = 90°$.

In order to investigate the effect of nanosphere radius, volume fraction, and length of the aperture in top gold layer, our simulations are executed with different geometry values. The real and imaginary parts of the effective permittivity of the TiN-nanosphere/LC hybrid for $\phi = 90°$ and radii of 5, 10, and 15 nm are demonstrated in Fig. 6.

It can be seen that the resonance of the TiN-nanosphere/LC hybrid remains the same by varying the nanosphere radius and only there is a small change in the amplitude of the resonance. Therefore, the radius of nanospheres is not considered as a degree of freedom to tune the absorber. The absorption spectra for different nanosphere radii are depicted in Fig. 7.

The real and imaginary parts of the effective permittivity for different values of volume fraction (p) are shown in Fig. 8.

The amplitude of the LC nanocomposite resonance is enhanced as the concentration of the TiN-nanospheres is increased.

It is worth noting that as the volume fraction increases, the real part of the nanocomposite permittivity is decreased at the wavelengths near 0.7 μm. The decrement of the TiN-nanosphere/LC hybrid permittivity causes a blue shift in the absorption peaks that are smaller than 0.7 - μm wavelengths. However, there is a red shift for the absorption wavelengths greater than 0.7 μm. The absorption spectra for the mentioned volume fractions are shown in Fig. 9.

The length of the aperture in the top gold layer is one of the most important factors in the design of the proposed structure. The absorption spectra for different square lengths are depicted in Fig. 10. The absorption behavior of the structure is changed by different values of the aperture length. When $a = 150$ nm, there are three more than 90% absorption peaks in the absorption spectrum. For the case of $a = 200$ nm, also, there are three absorption peaks but the absorption is decreased to 75%. The structure has two absorption peaks as $a = 250$ nm that are lower than 90%.
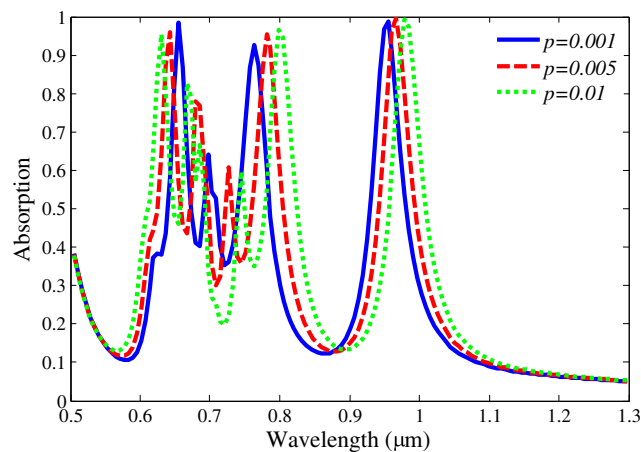

Fig. 9 The absorption spectra for $p = 0.001$, $p = 0.005$, and $p = 0.01$ as $\phi = 90°$, $a = 150$ nm, and $r = 10$ nm
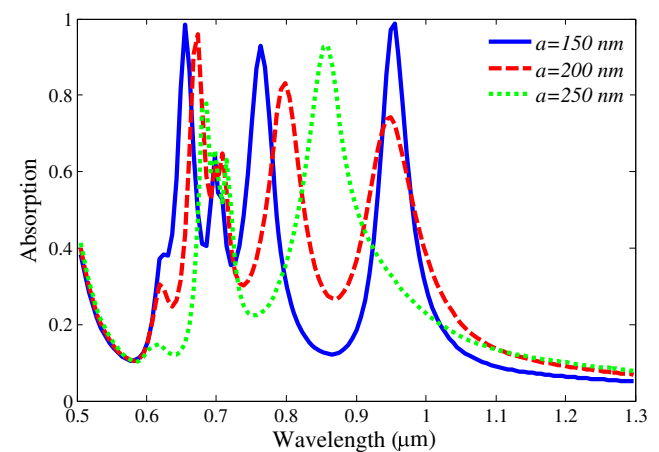

Fig. 10 The absorption spectra for different aperture lengths when $\phi = 90°$, $p = 0.001$, and $r = 10$ nm
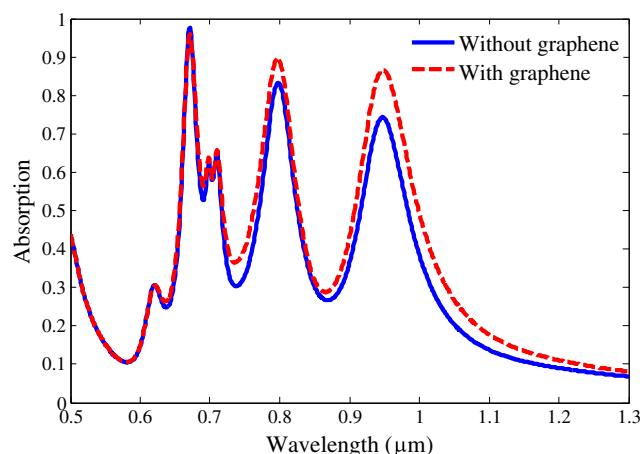
Fig. 11 The absorption spectra of the structure of Fig. 1 as a single sheet of graphene with $\mu_c = 0.15$ is used on the silica layer sandwiched between top gold layer and LC nanocomposite when $\phi = 90°$, $a = 200$ nm, $r = 10$ nm, and $p = 0.001$

The absorption of the structure can be enhanced by utilizing a single sheet of graphene on the silica layer, as shown in Fig. 11. The light and graphene interaction is influenced by the near field enhancement of LSP created on the TiN-nanospheres. In other words, LSPR of TiN-nanospheres boosts the light absorption in graphene, so the absorption value of the whole structure is enhanced to 90% due to the light and graphene interaction.

Conclusion

In this paper, a tunable plasmonic absorber based on TiN-nanosphere/liquid crystal (LC) nanocomposite is studied. It is shown that the flexible property of LC permittivity plays a great role to make the device tunable. In addition, volume fraction is another degree of freedom to make the absorber tunable. The nanosphere radius of the nanocomposite structure is not considered as a parameter to tune the absorber due to its insignificant effect. The length of the top aperture is another parameter of the structure which is decisive. Overall, the proposed absorber has three more that 90% absorption peaks at visible and near-infrared wavelengths. Moreover, it is shown that the decrement of the absorption caused by the structure dimensions can be compensated by a single sheet of graphene over the nanocomposite.

References

1. Meshram M, Agrawal NK, Sinha B, Misra P (2004) Characterization of M-type barium hexagonal ferrite-based wide band microwave absorber. J Magn Magn Mater 271(2-3):207–214. https://doi.org/10.1016/j.jmmm.2003.09.045

2. Landy NI, Sajuyigbe S, Mock J, Smith D, Padilla W (2008) Perfect metamaterial absorber. Phys Rev Lett 100(20):207402. https://doi.org/10.1103/PhysRevLett.100.207402

3. Hao J, Wang J, Liu X, Padilla WJ, Zhou L, Qiu M (2010) High performance optical absorber based on a plasmonic metamaterial. Appl Phys Lett 96(25):251104. https://doi.org/10.1063/1.3442904

4. Wang Y (1995) Voltage induced color selective absorption with surface plasmons. Appl Phys Lett 67(19):2759–2761. https://doi.org/10.1063/1.114584

5. Liu N, Mesch M, Weiss T, Hentschel M, Giessen H (2010) Infrared perfect absorber and its application as plasmonic sensor. Nano Lett 10(7):2342–2348. https://doi.org/10.1021/nl9041033

6. Tittl A, Mai P, Taubert R, Dregely D, Liu N, Giessen H (2011) Palladium-based plasmonic perfect absorber in the visible wavelength range and its application to hydrogen sensing. Nano Lett 11(10):4366–4369. https://doi.org/10.1021/nl202489g

7. Aydin K, Ferry VE, Briggs RM, Atwater HA (2011) Broadband polarization-independent resonant light absorption using ultrathin plasmonic super absorbers. Nat Commun 2:1–7. https://doi.org/10.1038/ncomms1528

8. Cai Y, Zhu J, Liu QH, Lin T, Zhou J, Ye L, Cai Z (2015) Enhanced spatial near-infrared modulation of graphene-loaded perfect absorbers using plasmonic nanoslits. Opt Express 23(25):32318–32328. https://doi.org/10.1364/OE.23.032318

9. Kang Z, Guo X, Jia Z, Xu Y, Liu L, Zhao D, Qin G, Qin W (2013) Gold nanorods as saturable absorbers for all-fiber passively Q-switched erbium-doped fiber laser. Opt Mater Express 3(11):1986–1991. https://doi.org/10.1364/OME.3.001986

10. Si G, Zhao Y, Leong ESP, Liu YJ (2014) Liquid-crystal-enabled active plasmonics: a review. Materials 7(2):1296–1317. https://doi.org/10.3390/ma7021296

11. Taylor T, Arora S, Fergason J (1970) Temperature-dependent tilt angle in the smectic C phase of a liquid crystal. Phys Rev Lett 25(11):722–726. https://doi.org/10.1103/PhysRevLett.25.722

12. Isić G, Vasić B, Zografopoulos DC, Beccherelli R, Gajić R (2015) Electrically tunable critically coupled terahertz metamaterial absorber based on nematic liquid crystals. Phys Rev Appl 3(6):064007. https://doi.org/10.1103/PhysRevApplied.3.064007

13. Su Z, Yin J, Zhao X (2015) Soft and broadband infrared metamaterial absorber based on gold nanorod/liquid crystal hybrid with tunable total absorption. Sci Rep 5(1):16698. https://doi.org/10.1038/srep16698

14. Spector M, Heiney P, Naciri J, Weslowski B, Holt D, Shashidhar R (2000) Electroclinic liquid crystals with large induced tilt angle and small layer contraction. Phys Rev E 61(2):1579–1584. https://doi.org/10.1103/PhysRevE.61.1579

15. Zhao Y, Hao Q, Ma Y, Lu M, Zhang B, Lapsley M, Khoo IC, Jun Huang T (2012) Light-driven tunable dual-band plasmonic absorber using liquid-crystal-coated asymmetric nanodisk array. Appl Phys Lett 100(5):053119. https://doi.org/10.1063/1.3681808

16. Fusco V, Cahill R, Hu W, Simms S (2008) Ultra-thin tunable microwave absorber using liquid crystals. Electron Lett 44(1):37–38. https://doi.org/10.1049/el:20082191

17. Shrekenhamer D, Chen W-C, Padilla WJ (2013) Liquid crystal tunable metamaterial absorber. Phys Rev Lett 110(17):177403. https://doi.org/10.1103/PhysRevLett.110.177403

18. Sihvola AH, Kong JA (1988) Effective permittivity of dielectric mixtures. IEEE Trans Geosci Remote 26:420–429. https://doi.org/10.1109/36.3045

19. Garnett JM (1906) Colours in metal glasses, in metallic films, and in metallic solutions. II. Philos Trans R Soc Lond 76(387-401):370–373. https://doi.org/10.1098/rsta.1906.0007

20. Garcıa M, Llopis J, Paje S (1999) A simple model for evaluating the optical absorption spectrum from small Au-colloids in sol–gel films. Chem Phys Lett 315(5-6):313–320. https://doi.org/10.1016/S0009-2614(99)01206-3

21. Granqvist C, Hunderi O (1978) Conductivity of inhomogeneous materials: effective-medium theory with dipole-dipole interaction. Phys Rev B 18(4):1554–1561. https://doi.org/10.1103/PhysRevB.18.1554

22. Gao D, Gao L (2010) Goos–Hänchen shift of the reflection from nonlinear nanocomposites with electric field tunability. Appl Phys Lett 97(4):041903. https://doi.org/10.1063/1.3470000

23. Yang Y, Wang W, Boulesbaa A, Kravchenko II, Briggs DP, Puretzky A, Geohegan D, Valentine J (2015) Nonlinear fano-resonant dielectric metasurfaces. Nano Lett 15(11):7388–7393. https://doi.org/10.1021/acs.nanolett.5b02802

24. Gao D, Gao H, Qiu CW (2011) Birefringence-induced polarization-independent and nearly all-angle transparency through a metallic film. EPL-Europhys Lett 95:34004. https://doi.org/10.1209/0295-5075/95/34004

25. Geim AK, Novoselov KS (2007) The rise of graphene. Nat Mater 6(3):183–191. https://doi.org/10.1038/nmat1849

26. Nair RR, Blake P, Grigorenko AN, Novoselov KS, Booth TJ, Stauber T, Peres NMR, Geim AK (2008) Fine structure constant defines visual transparency of graphene. Science 320(5881):1308–1308. https://doi.org/10.1126/science.1156965

27. Alaee R, Farhat M, Rockstuhl C, Lederer F (2012) A perfect absorber made of a graphene micro-ribbon metamaterial. Opt Express 20(27):28017–28024. https://doi.org/10.1364/OE.20.028017

28. Thongrattanasiri S, Koppens FH, De Abajo FJG (2012) Complete optical absorption in periodically patterned graphene. Phys Rrev Lett 108(4):047401. https://doi.org/10.1103/PhysRevLett.108.047401

29. Yao G, Ling F, Yue J, Luo C, Ji J, Yao J (2016) Dual-band tunable perfect metamaterial absorber in the THz range. Opt Express 24(2):1518–1527. https://doi.org/10.1364/OE.24.001518

30. Zhao B, Zhao J, Zhang Z (2014) Enhancement of near-infrared absorption in graphene with metal gratings. Appl Phys Lett 105(3):031905. https://doi.org/10.1063/1.4890624

31. Lu H, Cumming BP, Gu M (2015) Highly efficient plasmonic enhancement of graphene absorption at telecommunication wavelengths. Opt Lett 40(15):3647–3650. https://doi.org/10.1364/OL.40.003647.

32. Zare MS, Nozhat N, Rashiditabar R (2016) Improving the absorption of a plasmonic absorber using a single layer of graphene at telecommunication wavelengths. Appl Opt 55(34):9764–9768. https://doi.org/10.1364/AO.55.009764

33. Zare MS, Nozhat N, Rashiditabar R (2017) Tunable graphene based plasmonic absorber with grooved metal film in near infrared region. Opt Commun 398:56–61. https://doi.org/10.1016/j.optcom.2017.04.025.

34. Naik GV, Schroeder JL, Ni X, Kildishev AV, Sands TD, Boltasseva A (2012) Titanium nitride as a plasmonic material for visible and near-infrared wavelengths. Opt Mater Express 2(4):478–489. https://doi.org/10.1364/OME.2.000478

35. Li J, Wu S-T, Brugioni S, Meucci R, Faetti S (2005) Infrared refractive indices of liquid crystals. J Appl Phys 97(7):073501. https://doi.org/10.1063/1.1877815

36. Khoo I, Werner D, Liang X, Diaz A, Weiner B (2006) Nanosphere dispersed liquid crystals for tunable negative-zero-positive index of refraction in the optical and terahertz regimes. Opt Lett 31(17):2592–2594. https://doi.org/10.1364/OL.31.002592

37. Asadi R, Malek-Mohammad M, Khorasani S (2011) All optical switch based on Fano resonance in metal nanocomposite photonic crystals. Opt Commun 284(8):2230–2235. https://doi.org/10.1016/j.optcom.2010.12.085

38. Reinholdt A, Pecenka R, Pinchuk A, Runte S, Stepanov A, Weirich TE, Kreibig U (2004) Structural, compositional, optical and colorimetric characterization of TiN-nanoparticles. Eur Phys J D-At Mol Opt Plasma Phys 31(1):69–76. https://doi.org/10.1140/epjd/e2004-00129-8

39. Johnson PB, Christy R-W (1972) Optical constants of the noble metals. Phys Rev B 6(12):4370–4379. https://doi.org/10.1103/PhysRevB.6.4370

40. Pflüger J, Fink J, Weber W, Bohnen K, Crecelius G (1984) Dielectric properties of TiC x, TiN x, VC x, and VN x from 1.5 to 40 eV determined by electron-energy-loss spectroscopy. Phys Rev B 30(3):1155–1163. https://doi.org/10.1103/PhysRevB.30.1155

41. Gao L, Lemarchand F, Lequime M (2012) Exploitation of multiple incidences spectrometric measurements for thin film reverse engineering. Opt Express 20(14):15734–15751. https://doi.org/10.1364/OE.20.015734

42. Hibbins AP, Sambles JR, Lawrence CR (1998) Surface plasmon-polariton study of the optical dielectric function of titanium nitride. J Mod Opt 45(10):2051–2062. https://doi.org/10.1080/09500349808231742

43. Patsalas P, Logothetidis S (2001) Optical, electronic, and transport properties of nanocrystalline titanium nitride thin films. J Appl Phys 90(9):4725–4734. https://doi.org/10.1063/1.1403677

44. Hanson GW (2008a) Dyadic Green's functions and guided surface waves for a surface conductivity model of graphene. J Appl Phys 103(6):064302. https://doi.org/10.1063/1.2891452

45. Hanson GW (2008b) Dyadic Green's functions for an anisotropic, non-local model of biased graphene. IEEE T Antenn Propag 56(3):747–757. https://doi.org/10.1109/TAP.2008.917005

46. Yang D-K (2014) Fundamentals of liquid crystal devices. John Wiley & Sons, Hoboken. https://doi.org/10.1002/9781118751992